Single-cell analysis of the dynamics and functional outcomes of interactions between human natural killer cells and target cells

Title:

Single-cell analysis of the dynamics and functional outcomes of interactions between human natural killer cells and target cells

Authors:

Yvonne J. Yamanaka,[1] Christoph T. Berger,[2] Magdalena Sips,[2] Patrick C. Cheney,[2] Galit Alter,[2] and J. Christopher Love[2-4]

Affiliations:

1. Department of Biological Engineering, Massachusetts Institute of Technology, 77 Massachusetts Ave., Cambridge, MA 02139

2. The Ragon Institute of MGH, MIT, and Harvard, Charlestown Navy Yard, Boston, MA 02129

3. Department of Chemical Engineering, Massachusetts Institute of Technology, 77 Massachusetts Ave., Cambridge, MA 02139

4. Koch Institute for Integrative Cancer Research, 77 Massachusetts Ave., Bldg. 76-253, Cambridge, MA 02139

Corresponding author:

J. Christopher Love, Ph.D.
Department of Chemical Engineering
Koch Institute for Integrative Cancer Research
Massachusetts Institute of Technology
77 Massachusetts Ave., Bldg. 76-253
Cambridge, MA 02139
Phone: 617-324-2300
Fax: 617-258-5042
Email: clove@mit.edu

Graphical abstract

We used arrays of subnanoliter wells (nanowells) to monitor the dynamics of individual NK cell-target cell interactions and quantify the resulting cytolytic and secretory responses.

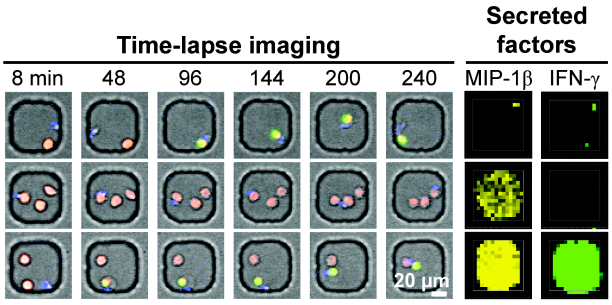

Insight statement

The cytolytic and secretory activities of natural killer (NK) cells are important components of the innate immune response against potentially harmful target cells. We developed a nanowell-based platform to efficiently acquire multiparametric measurements of encounters between individual NK cells and tumor target cells. The integrated profiles of contact behavior, motility, lysis, and secretion yielded new insights into the heterogeneities and correlations of these parameters at the single-cell level. We found that NK cells lyse targets in an autonomous, history-dependent manner, and that the target cell-induced secretory activity of individual NK cells associated with their migratory characteristics. This technology can be adapted to investigate, with single-cell resolution, the dynamic and functional attributes of other cellular systems of interest.

Abstract

Natural killer (NK) cells are a subset of innate immune lymphocytes that interrogate potential target cells and rapidly respond by lysing them or secreting inflammatory immunomodulators. Productive interactions between NK cells and targets such as tumor cells or virally infected cells are critical for immunological control of malignancies and infections. For individual NK cells, however, the relationship between the characteristics of these cell-cell interactions, cytolysis, and secretory activity is not well understood. Here, we used arrays of subnanoliter wells (nanowells) to monitor individual NK cell-target cell interactions and quantify the resulting cytolytic and secretory responses. We show that NK cells operate independently when lysing a single target cell and that lysis is most probable during an NK cell's first encounter with a target. Furthermore, we demonstrate that the secretion of interferon-γ (IFN-γ) occurs most often among NK cells that become the least motile upon contacting a target cell but is largely independent of cytolysis. Our findings demonstrate that integrated analysis of the cell-cell interaction parameters, cytolytic activity, and secretory activity of single NK cells can reveal new insights into how these complex functions are related within individual cells.

Introduction

Natural killer (NK) cells are granular lymphocytes classically defined by their capacity to recognize and kill tumor or virally infected cells without the need for antigen sensitization. They can also secrete cytokines and chemokines that promote the induction of a robust immune response.[1,2] NK cells identify target cells using a variety of activating and inhibitory germline-encoded surface receptors.[3,4] The integration of signals from these receptors regulates the cells' cytolytic and secretory responses.[5-9] In addition, cytokines such as interleukin-2 (IL-2) from T cells,[10-13] interferon-α (IFN-α) from plasmacytoid dendritic cells (pDCs),[14] and IL-12, IL-15, and IL-18 from macrophages and DCs[15-19] can significantly enhance cytotoxicity and secretion of cytokines from NK cells.

Recent data have shown that NK cells perform several contact-dependent immunomodulatory functions in addition to directly eliminating target cells.[2] For example, NK cells can tune the development of antiviral adaptive immunity by eliminating virus-infected DCs,[20] by maturing and 'editing' pools of DCs to optimize antigen presentation,[21,22] or by lysing and suppressing activated T cells.[23,24] In these regulatory interactions, as well as in direct interactions with target cells, the efficacy of the NK cell-mediated immune response is determined by the cytolytic and secretory decisions that each NK cell makes upon encountering another cell. The direct relationship between cell-contact parameters, cytolysis, and the secretion of cytokines is challenging to study, however, due to the large cell-to-cell variability in both the functional capacities of NK cells[1,7,15,25-27] and the dynamics of NK cell interactions (e.g., duration of conjugation, time to lysis, motility).[28-32]

This functional diversity motivates the study of NK cell-mediated cytolysis, secretion, and interaction dynamics for individual NK cells. Conventional technologies, however, cannot efficiently match observations of these traits with single-cell resolution. Standard microscopy-based approaches offer sub-cellular imaging resolution of cell-cell interactions but are limited in throughput and are not amenable to measuring cytokine production from untransfected human cells. Lysispot/ELISpot assays enable the concurrent detection of cytolysis and secretion[33] but are not conducive to monitoring interactions over time. Finally, flow cytometry, combined with intracellular cytokine staining (ICS), provides robust measures of the phenotypic and functional attributes of large numbers of single NK cells but de-couples the history of cell-cell interactions from the functional readout.

Multiple functional properties of NK cells can be measured at the single-cell level by isolating and monitoring individual NK cells in submicroliter wells (microwells) or subnanoliter wells (nanowells). This approach has been used to demonstrate that the lysis of 293T target cells colocalized with IL-2-activated primary human NK cells in nanowells occurs with diverse dynamics—some targets display a rapid loss of calcein (a live-cell dye) when they are lysed by an NK cell, some display a slow loss of calcein, and others remain unlysed despite being contacted by an NK cell.[30] Analyses in microwells have also shown that individual primary human NK cells undergo dynamic changes in their migratory behavior by transitioning between directed migration, random migration, and periods of transient arrests in migration.[32]

Microscopy-based assays using micro- and nanowells are well suited for monitoring cytolytic activity and motility, but to date there has not been an analytical process that directly integrates the measurement of these dynamic behaviors with other functional outcomes, such as secretory activity, at the single-cell level. Because one of the primary functions of NK cells is to secrete cytokines that orchestrate immune responses to pathogens and malignant cells,[1,2] we developed a nanowell-based approach to concomitantly relate the secretory activity of individual NK cells to the dynamics of their interactions with target cells. Using this integrated process, we monitored hundreds of isolated NK cell-target cell interactions in parallel and analyzed the relationship between cytolytic activity, secretory activity, and motility. We found that the acute secretion of IFN-γ from an NK cell is associated with its motility during contact with the target cell but is not associated with the cytolytic outcome of the encounter.

Methods

Cells and stimulations

Human peripheral blood mononuclear cells (PBMCs) were isolated from whole blood by Ficoll-Hypaque (Sigma-Aldrich) gradient centrifugation. Study subjects were drawn from a healthy donor cohort at the Massachusetts General Hospital in Boston. The Partners Healthcare Institutional Review Board and the Massachusetts Institute of Technology Committee on the Use of Humans as Experimental Subjects approved the study, and each subject gave written informed consent. NK cells were isolated from PBMCs by negative selection (EasySep Human NK Cell Enrichment Kit; STEMCELL Technologies) and maintained in complete media (RPMI 1640 (Mediatech) supplemented with 10% heat-inactivated fetal bovine serum (PAA), 2 mM L-glutamine, 100 U/mL penicillin, 100 μg/mL streptomycin, and 10 mM HEPES buffer (all from Mediatech)). Where indicated, NK cells were stimulated with IL-2 (50 U/mL; NIH AIDS Research & Reference Reagent Program), IFN-α (10 ng/mL; PBL InterferonSource), IL-12 (10 ng/mL), IL-15 (100 ng/mL), or IL-18 (100 ng/mL) (all from R&D Systems). The major histocompatibility complex (MHC) class I-deficient K562 cell line (ATCC) was maintained in complete media and used as a model target cell.

Fabrication of nanowell arrays

Arrays of poly(dimethylsiloxane) (PDMS; Dow Corning) nanowells containing either 30 μm or 50 μm cubic wells were prepared by injection molding, as described previously[34-36] and in the Supplemental Methods.

Single-cell cytolysis assay and video microscopy

The single-cell cytolysis (SCC) assay was adapted from an assay we recently developed to identify antigen-specific cytolytic $CD8^+$ T cells.[36] The assay operates by loading small groups (~1–5 cells/well) of effector and target cells on an array of nanowells and observing the cytolytic encounters that occur in each well (Fig. 1A). Fluorescently labeled NK cells (calcein violet, 1 μM; Invitrogen, or for video microscopy, eFluor 670, 0.5 μM; eBioscience) and target cells (CellTracker Red, 2.5 μM; Invitrogen) were adjusted to a density of 5×10^5 cell/mL and loaded onto the arrays. Arrays with 30 μm or 50 μm cubic wells were used to favor the loading of single or multiple targets per well, respectively. Media containing SYTOX green (nucleic acid stain to

identify dead cells, 0.5 μM; Invitrogen) was applied and the arrays were covered with lifter slips (Electron Microscopy Sciences) or glass slides.

Arrays were imaged using an automated inverted epifluorescence microscope (Axio Observer; Carl Zeiss, 10x/0.3 objective) fitted with an EM-CCD camera (ImagEM; Hamamatsu). For the SCC assay, images were collected at 0 h to determine the initial occupancy of each well and at 4 h to validate the occupancy and determine the acquisition of SYTOX by targets. Arrays were incubated at 37°C and 5% CO_2 between the initial and final images. Video microscopy was performed in a similar manner by imaging a subsection of the array at 8 min intervals over a total of 4 h. A custom-written script[35] was used to process the images.

Microengraving to detect secreted proteins

The secretion of cytokines and chemokines from the cells residing in each nanowell was measured by microengraving using previously reported protocols.[34-39] Microengraving measures secretory events from both single- and multi-celled wells, but it does not directly attribute secretions from multi-celled wells to specific cells within the well. (The cells' respective contributions may be deconvolved based on independently determined knowledge of cellular properties (e.g., certain cells do not secrete specific analytes under certain conditions).) Secreted macrophage inflammatory protein-1β (MIP-1β, or CC chemokine ligand 4 (CCL4)) and interferon-γ (IFN-γ) from each well were captured for 1 h (30 μm wells) or 2 h (50 μm wells) on a glass slide coated with the corresponding capture antibodies (Fig. 4A). The resulting microarray of captured proteins was then probed with fluorescent detection antibodies and imaged. See Supplemental Methods for additional details.

Functional and phenotypic flow cytometry

For the functional flow cytometric assays, 10^6 PBMCs were pre-incubated in the presence or absence of stimulatory cytokines (as indicated in the text), and then incubated with K562 target cells at an effector:target (PBMC:K562) ratio of 10:1 in the presence of 0.5 μg/mL Brefeldin A (Sigma-Aldrich), 0.3 μg/mL Monensin (Golgi-Stop, BD Biosciences), and anti-CD107a-PE-Cy5 antibody (BD Biosciences). After 4 h of incubation, cells were stained using the LIVE/DEAD Fixable Blue Dead Cell Stain (Invitrogen), washed, and then incubated for 15 min with the following antibodies: anti-CD3-Pacific Blue (PB), anti-CD14-PB, anti-CD19-PB, anti-CD16-

allophycocyanin (APC)-Cy7, and anti-CD56-phycoerythrin (PE)-Cy7 (all BD Biosciences). Cells were then fixed and permeabilized using the Cytofix/Cytoperm solution kit (BD Biosciences) according to the manufacturer's instructions. Intracellular cytokine staining was performed for 30 min with anti-IFN-γ-fluorescein isothiocyanate (FITC) and anti-MIP-1β-PE (both BD Biosciences). To assess how the different stimulation conditions might affect the phenotypes and activation states of NK cells, PBMCs were separately stained with the immunophenotypic markers anti-NKG2D-APC, anti-NKp46-PE (both BD Biosciences), anti-CD69-FITC, and anti-perforin-peridinin chlorophyll protein (PerCP)-Cy5.5 (both eBioscience). In all experiments, NK cells were defined as live $CD3^-CD14^-CD19^-$ lymphocytes expressing CD56 and/or CD16 (Fig. S1). In separate experiments, surface expression of NKG2D ligands on K562 cells was confirmed using anti-UL16 binding protein (ULBP)-1-PE, anti-ULBP-2-PE, anti-ULBP-3 (primary) (all from R&D Systems) with goat anti-mouse-APC (secondary), and MHC class I chain-related protein A/B (MICA/B)-PE (both BD Biosciences) (Fig. S2). Data were acquired on a BD LSRII (BD Biosciences) flow cytometer and analyzed using FlowJo software (V9.3.1; Tree Star).

Data analysis

Raw data were processed as described above and in the Supplemental Methods. In all experiments, the wells that were located on the edge of the array were excluded from analysis to minimize any potential edge effects. To analyze the video microscopy data, a custom-written MATLAB (R2010b; MathWorks) script was used to calculate parameters describing the interactions of single NK cells with up to four target cells. Intervals of NK cell-target cell contact were manually verified. Custom-written MATLAB scripts were used to correlate data from the SCC assay or video microscopy with data from microengraving on a per-well basis. Statistical analyses were performed with Prism 5 (GraphPad Software); specific statistical tests are indicated in the text.

Results

Individual NK cells lyse target cells when co-incubated in nanowells

We developed a single-cell cytolysis (SCC) assay to directly measure the cytolytic behavior of thousands of individual NK cells (Fig. 1A). NK cells and K562 target cells were co-deposited onto an array of 30 μm cubic nanowells to obtain small, isolated groups of cells. The stochastic loading procedure resulted in the majority of the nanowells being filled with 0–3 cells of each type (Fig. S3). For the SCC assay, analysis was restricted to the 1,000–5,000 wells per array that contained exactly one NK cell and one target cell. After 4 h of co-incubation in the nanowells, productive cytolytic interactions were identified by the appearance of $SYTOX^+$ target cells (Fig. 1A–B). These initial experiments established that thousands of cytolytic and non-cytolytic interactions between individual NK cells and targets could be observed in parallel.

The cytolytic potential of NK cells is strongly modulated by cytokines that are released locally during an immune response.[11-14,17-19] We therefore assessed how stimulation with exogenous cytokines affected the cytolysis measured in the SCC assay (Fig. 1C). Prior to the assay, NK cells were incubated for 20 h with media, IL-2, IFN-α plus IL-2, or a combination of IL-12, IL-15, and IL-18. In the absence of cytokine stimulation, 7% ± 6% of NK cells in nanowells containing a single NK cell and a single target lysed the target. In each experiment, this rate was significantly above the 2% ± 1% background death rate of single target cells on the same array ($P < .0001$, Chi-squared with Yate's correction). Activation of NK cells with exogenous cytokines prior to the assay resulted in a significant increase in the frequency of target cell death (23–26%) compared with unstimulated NK cells ($P < .05$, one-way analysis of variance (ANOVA) followed by Tukey's post-test) (Fig. 1C).

The cytolytic potential of NK cells[40] and T cells[41] is associated with target cell-induced surface expression of CD107a, a degranulation marker. Assays employing flow cytometry commonly use CD107a as a surrogate measurement for the cytolytic activity of single NK cells.[40] We therefore compared the frequency of single-cell cytolysis (measured by the SCC assay) with the frequency of NK cells expressing CD107a after 4 h of co-incubation with targets (measured by flow cytometry) (Fig. 1C). For each stimulation condition, the frequency of NK cells that upregulated CD107a expression was higher than the frequency of cytolytic NK cells observed in the SCC assay, but the two measurements were significantly correlated ($R^2 = 0.89$, $P < .05$, Pearson correlation). The discrepancy in the absolute frequencies may be explained by

differences in bulk compared to single-cell stimulation, by the fact that CD107a can be expressed on the surface of NK cells that have been activated but have not lysed a target,[40] or by the fact that the acquisition of SYTOX signal marks the end-stages of target cell death (membrane permeabilization). Overall, these results demonstrated that the SCC assay monitors the cytolytic outcome of thousands of individual NK cell-target cell pairs, and that the cytolytic frequencies measured in this assay reflect the cytolytic activity as measured in bulk cultures.

Small groups of NK cells do not cooperate to kill single target cells

We next quantified the frequency of cytolysis in nanowells containing different numbers of NK cells (zero, one, two, or three NK cells) in the presence of a single target to determine whether NK cells kill more efficiently in groups than in isolation (Fig. 2A). As expected, increasing the number of NK cells in the well led to increased frequencies of cytolysis. To determine whether this increase occurred in a cooperative or independent manner, we tested if the observed frequency of lysis in wells containing one NK cell could predict the frequency of lysis in wells containing multiple NK cells. If NK cells act independently when killing a single target, then the predicted frequency of dead targets in wells with n NK cells is $1 - (1 - P_{death})^n$, where P_{death} is the frequency (probability) of the target cell being lysed when co-located with a single NK cell. We found that the observed frequencies of lysis in wells with multiple NK cells were not significantly different from the predicted frequencies ($P > .05$ for 23 of the 24 cases tested, Fisher's exact test) (Fig. 2B). This result suggested that NK cells residing in small groups in nanowells operate independently to mediate the acute lysis of a single target cell; in other words, they do not attack more effectively as a group than as individuals (e.g., by enhancing the cytolytic behavior of neighboring NK cells or by delivering partial lytic hits that cumulatively, but not individually, result in lysis). We note that cooperative effects over larger length scales *in vivo* could occur by the selective recruitment of specific subsets of NK cells to the site of infection or tumorigenesis.

IL-2-activated NK cells lyse target cells with heterogeneous dynamics and in an order-dependent manner

The induction of functional responses in NK cells depends heavily on the dynamics of contact between NK cells and the target cells that they interrogate.[28,29] To characterize the dynamics of

contact, we performed time-lapse microscopy on a subsection of the array to collect movies of single NK cells interrogating 0–4 target cells in 50 μm cubic wells (Fig. 3A and Supplementary Videos 1–4). NK cells were stimulated for 44 h in 50 U/mL IL-2 prior to the assay to ensure a robust functional response. This stimulation activated NK cells (47% ± 9% $CD69^+$), but did not change the expression of NKp46, NKG2D, or perforin compared with unstimulated NK cells (Fig. S4).

NK cells patrolled the nanowells and formed multiple contacts with targets in the wells (Fig. 3B). NK cells that formed contacts with targets mediated the cytolysis of one or more targets in 25% of the cases (81 out of 324, compiled from two donors). Among cytolytic NK cells, the duration of contact with a target prior to lysis (marked by membrane permeabilization) ranged from less than 8 min to over 200 min (Fig. 3C). This wide distribution in times implies that the initiation and execution of cytolytic activity following contact with a target occurs with heterogeneous dynamics.

The probability of a target cell being lysed depended upon the order in which it was contacted by the NK cell—the first target that an NK cell encountered was more likely to be lysed than targets that were encountered subsequently (Fig. 3D). A decrease in cytolytic activity over sequential encounters with target cells could occur if the cytolytic potential of an NK cell is diminished after the delivery of a lytic hit. To test this hypothesis, we examined whether NK cells that lysed the first target they encountered were able to lyse other target cells upon subsequent contact. Among the NK cells that contacted 2–4 target cells, 27% (37 out of 135) lysed the first target that they encountered. Within the group of cells that exhibited cytolytic activity upon the first encounter, 19% (7 out of 37) also lysed additional targets that they encountered later (e.g., Supplementary Video 4). This result suggested that NK cells retain their cytolytic potential after delivering a lytic hit (consistent with previous reports of serial killing[31] and bulk studies demonstrating that NK cells retain perforin and granzyme loading after target cell-induced degranulation[42]), but that only a subset of the initially cytolytic NK cells proceed to serially lyse multiple targets. In addition, among the group of NK cells that did not lyse the first target, 93% (92 out of 98) also did not lyse any of the other targets that they subsequently encountered. This result demonstrated that NK cells that do not lyse the first target they encounter are unlikely to exhibit cytolytic activity upon subsequent encounters with similar target cells within short periods (4 h). Together, these results suggest that the decrease in

cytolytic activity over sequential encounters with target cells occurs because (1) only a fraction of NK cells that lyse the first target they encounter continue on to lyse additional targets, and (2) NK cells that do not lyse the first target they encounter are unlikely to lyse targets that they encounter later.

Microengraving measures the short-term secretory activity of individual NK cells

In addition to their cytolytic activity, NK cells also contribute to immune control by secreting cytokines and chemokines. We used microengraving, a technique to detect the proteins that are secreted by the cells residing within each nanowell on the array (Fig. 4A),[34-39] to measure the short-term secretory profiles of individual NK cells and match them to the corresponding observations of the NK cell-target cell interactions (Fig. 4B). We focused our analysis on the secretion of MIP-1β and IFN-γ. These proteins are secreted by NK cells and play important roles in coordinating the immune response. MIP-1β is a chemokine that can attract NK cells[43] and other immune cells; it also suppresses human immunodeficiency virus (HIV) infection by inhibiting the binding of HIV to CC chemokine receptor type 5 (CCR5).[44,45] IFN-γ is a cytokine that inhibits viral replication, increases the presentation of antigen, and polarizes the differentiation of T helper cells to the Th1 lineage.[46]

We first validated that microengraving could detect characteristic patterns of secretory activity from NK cells that interacted with target cells. Prior to microengraving, NK cells were incubated for 20 h in either media alone or a combination of IL-12, IL-15, and IL-18. NK cells were then loaded with target cells into 30 μm cubic nanowells and incubated for 4 h to allow interactions with targets to take place. Following incubation, microengraving was performed for 1 h to capture secreted MIP-1β and IFN-γ, and wells that contained a single NK cell and multiple target cells were analyzed for secretion (Fig. 4C). Previous reports have shown that, in the absence of activation with exogenous cytokines, MIP-1β is the dominant secretory product from NK cells that interact with K562 target cells.[7] Similarly, we found that MIP-1β was secreted by a small but consistently detectable fraction of NK cells that were cultured in media alone prior to being introduced to the target cells in the nanowells (Fig. 4C). NK cells that were activated with IL-12, IL-15, and IL-18 prior to the assay exhibited increased secretion of MIP-1β and strong secretion of IFN-γ. This finding was consistent with previous reports showing that IL-12, IL-15, and IL-18 activate NK cells and induce the secretion of cytokines, especially IFN-γ.[7,15,16]

Analogous assays performed using ICS in combination with flow cytometry produced similar trends in relative secretory activity (Fig. 4C). Together, these experiments confirmed that microengraving can be used to profile the secretion of MIP-1β and IFN-γ from NK cells interacting with target cells in the array of nanowells.

Secretion of IFN-γ from IL-2-activated NK cells is associated with reduced motility during contact with target cells

As a population, NK cells patrol their local microenvironment (e.g., lymph node or tissue), interrogate target cells, lyse target cells, and secrete cytokines. How these diverse functional parameters are related in each individual NK cell, however, has not been well characterized. To address this question, we matched observations of interactions (determined by time-lapse microscopy) between single IL-2-activated (50 U/mL, 44 h) NK cells and target cells in 50 μm cubic wells to measurements of secreted MIP-1β and IFN-γ collected via microengraving from the same nanowells (Fig. 5A). The resulting collection of functional profiles allowed us to quantitatively analyze cytolysis, secretion, and the dynamics of interaction in individual NK cells.

We first examined whether target cell-induced secretory activity and cytolytic activity were associated for individual NK cells. NK cells that contacted at least one target cell displayed robust secretion of MIP-1β and IFN-γ (Fig. 5B). Secretion was not observed in the absence of contact with a target, even if a target cell was present in the well. Among NK cells that contacted at least one target, however, there was no significant difference in the secretion of MIP-1β or IFN-γ between the cytolytic and non-cytolytic groups of NK cells (Fig. 5B). These results suggest that acute, target cell-induced secretory activity is not closely correlated to cytolytic activity in individual IL-2-activated NK cells.

To investigate how the dynamics of contact with target cells may regulate cytolysis and secretion in single NK cells, we next examined whether the motility of NK cells during contact with targets was associated with the subsequent cytolytic or secretory outcome of the encounter. The velocities of NK cells during periods of contact with target cells were reduced compared with the velocities in the absence of targets or after disengagement from a target (Fig. 5C; $P < .001$, Kruskal-Wallis test followed by Dunn's post-test). When the velocities of NK cells during contact with targets were further segregated based on the functional response (MIP-1$\beta^{-/+}$, IFN-γ^{-}

$^{/+}$, lysis$^{-/+}$), we found that cells that secreted IFN-γ had a significantly reduced velocity during contact with targets compared with cells that did not secrete IFN-γ (Fig. 5D; $P < .05$, Mann-Whitney test), and that these cells remained more arrested at the initial point of contact with the target (Fig. 5E). There was no significant difference between the during-contact velocities of NK cells that were segregated by the secretion of MIP-1β or cytolytic outcome (Fig. 5D). Together, these results suggest that NK cells receive stop signals of varying strengths after contacting a target, and that the degree of arrest in motility is related to the subsequent secretion of IFN-γ.

Discussion

NK cells induce cytolysis and secrete chemokines and cytokines in response to malignant or infected cells, and thus play a critical role in the immune control of cancer and infectious diseases.[2,47] Characterizing how individual NK cells interact with, and subsequently respond to, potential target cells is important for understanding the mechanisms by which they eliminate targets but leave healthy cells unharmed. Our group has recently described the use of arrays of nanowells to screen for HIV-specific $CD8^+$ T cells.[36] Here, we extended this approach to monitor interactions between individual NK cells and K562 target cells and then correlated these interactions to linked measurements of the cytolytic and secretory outcomes from the individual NK cells. The results of these dynamic, single-cell measurements begin to define the rules of engagement that modulate the functionality of NK cells during their response to target cells.

The unique ability of the SCC assay to precisely count the number of NK cells and targets in each nanowell allowed us to quantitatively investigate whether small groups of NK cells act cooperatively when killing an isolated target cell. Our results were consistent with a model in which each NK cell operates as a cytolytic agent that is independent of other NK cells present in the well. The lack of cooperative cytolytic behavior suggests that local paracrine signaling (over the sub-nanoliter volume of the well) between NK cells does not induce them to work synergistically to kill single target cells within a 4 h interval. This finding, however, does not eliminate the possibility for cooperative killing behavior among NK cells when killing multiple targets, killing resistant targets, or operating over larger length scales or longer intervals of time. Indeed, the bulk self-recruitment of NK cells into regions containing a high density of target cells is commonly observed.[48,49] In contrast, the self-recruitment of individual NK cells to aid in the acute elimination of a single target cell has been observed only on occasion,[50] thus supporting our finding that local cooperative behavior among NK cells is not a major mechanism by which the lysis of single, susceptible targets is achieved.

The variability in time to lysis that we observed may involve mechanisms by which NK cells progress through cytoskeletal polarization checkpoints before delivering a successful lytic hit[29] or cell-to-cell differences in the kinetics of apoptosis in targets.[51] NK cells lyse K562 target cells primarily by delivering perforin/granzyme-loaded cytolytic granules into the lytic synapse[52,53] rather than by triggering death receptor-mediated pathways of apoptosis induced by Fas ligand[54-56] (FasL) or tumor necrosis factor (TNF)-related apoptosis-inducing ligand[57]

(TRAIL). Some of the heterogeneity in lysis times and behaviors, however, could result from NK cells inducing the death of target cells by other mechanisms—for example, by using membrane nanotubes to facilitate cytolytic interactions with target cells.[58]

Our finding that cytolytic NK cells are most likely to lyse the first target cell they encounter suggests that they do not need to integrate activating signals collected during prior encounters with targets before overcoming the signaling threshold required for the delivery of a lytic hit; instead, they exert their cytolytic activity at the first opportunity. This pattern of activation is different from the pattern followed by T cells during priming in the lymph node under certain conditions, where it has been shown that the signals received through the T cell receptor are integrated over serial encounters with antigen-presenting cells until a threshold of activation is reached.[59] Because both the density and the type of ligands displayed by target cells have a large effect on the functional response of NK cells[5-7] it will be interesting to test whether different target cells produce different patterns of order-dependent cytolytic activity.

Cytolysis and secretion are the primary functions of NK cells during an immune response. By collecting linked measurements of the cytolytic and secretory activities of individual IL-2-activated NK cells upon exposure to target cells, we demonstrated that the acute secretion of IFN-γ and MIP-1β is not associated with the cytolytic status of NK cells. Studies using bulk mixtures of NK cells and target cells have also suggested that cytolysis and secretion may be differentially regulated or temporally distinct.[7,60-63] Furthermore, cytokines (e.g., IFN-γ, TNF) and perforin-loaded cytolytic granules are sorted into separate endosomes and released in distinct fashions from NK cells,[60] providing mechanistic support to the idea that cytolysis and secretion can be controlled independently within individual cells.

The relationship between the motility of NK cells and their secretory responses to target cells has not previously been analyzed at the single-cell level. Using integrated measurements of single, IL-2-activated NK cells, we found that target cell-induced secretion of IFN-γ was associated with the motility of the NK cells during contact with targets. The during-contact velocity of NK cells that secreted IFN-γ was significantly lower than that of NK cells that did not secrete IFN-γ. Previous reports have demonstrated that NK cells display a dose-dependent reduction in velocity when exposed to increasing concentrations of surface-bound MICA, an NKG2D ligand expressed on K562 target cells, and that these activating signals induce NK cells to arrest and form stable synapses with target cells.[28] It has also been shown that the level of

activation that is necessary to induce the secretion of IFN-γ is higher than that necessary to induce degranulation or the secretion of MIP-1β.[7] Our findings, therefore, are consistent with a model in which NK cells that receive the strongest activating signals upon encounter with a target have the lowest during-contact velocity (due to receiving a strong stop signal) and are also the most likely to surpass the signaling threshold required to induce the secretion of IFN-γ. A similar association between antigen-induced arrest and the secretion of IFN-γ has also been observed at the population level in mouse $CD4^+$ T cells.[64] Interestingly, we did not detect a significant difference in the during-contact motility of cells that did or did not secrete MIP-1β (a chemokine), although in other systems of interacting lymphocytes the secretion of chemokines has been shown to affect the characteristics of the immune synapse.[65] In general, the association between the during-contact velocity and the secretion of IFN-γ suggests that, for NK cells, there is overlap in the target cell-triggered signaling pathways that control motility and those that control the secretion of cytokines.

In summary, we have developed and validated a nanowell-based platform to quantitatively monitor and correlate the contact dynamics and functional outcomes (cytolysis, secretion) of interactions between individual NK cells and target cells. Integrated measurements such as these have not previously been possible to perform at the single-cell level due to the constraints of conventional assays. In the present study, we analyzed interactions between NK cells and tumor target cells, but the nanowell-based platform presented here could also be used to examine cross-regulation between NK cells and virally infected cells, DCs, or T cells with single-cell resolution. Moreover, the platform is suitable for use with samples containing a limited number of cells (10^4–10^5), and thus will enable unprecedented functional analysis of clinical biopsy specimens. Such applications could include the analysis of mucosal NK cells in HIV infection[66] or of intrahepatic NK cells in viral hepatitis.[67] In the current study, which focused on interactions between peripheral blood NK cells and K562 tumor target cells, we demonstrated that local cooperativity among NK cells does not contribute significantly to the lysis of single target cells, and that short-term secretory responses arising from individual NK cells are correlated with the dynamics of NK cell-target cell interactions but not cytolysis. Together, these results illustrate new properties by which NK cells perform immune surveillance and mediate the elimination of target cells.

Acknowledgments

The authors thank Q. Liu and E. Tkachenko for technical assistance; D. Irvine for comments on the manuscript; and N. Varadarajan and M. Foley for helpful discussions.

This work was supported by the Charles A. Dana Foundation, the W.M. Keck Foundation, and the Ragon Institute of MGH, MIT and Harvard. Y.J.Y was supported in part by a fellowship from the National Science Foundation and the Collamore-Rogers Fellowship. J.C.L. is a Latham Family Career Development Professor.

References

1. M. A. Cooper, T. A. Fehniger and M. A. Caligiuri, *Trends Immunol*, 2001, **22**, 633-640.
2. E. Vivier, E. Tomasello, M. Baratin, T. Walzer and S. Ugolini, *Nat Immunol*, 2008, **9**, 503-510.
3. L. L. Lanier, *Nat Immunol*, 2008, **9**, 495-502.
4. H. J. Pegram, D. M. Andrews, M. J. Smyth, P. K. Darcy and M. H. Kershaw, *Immunol Cell Biol*, 2010, **89**, 216-224.
5. Y. T. Bryceson, H. G. Ljunggren and E. O. Long, *Blood*, 2009, **114**, 2657-2666.
6. Y. T. Bryceson, M. E. March, H. G. Ljunggren and E. O. Long, *Blood*, 2006, **107**, 159-166.
7. C. Fauriat, E. O. Long, H. G. Ljunggren and Y. T. Bryceson, *Blood*, 2010, **115**, 2167-2176.
8. S. Mesecke, D. Urlaub, H. Busch, R. Eils and C. Watzl, *Sci Signal*, 2011, **4**, ra36.
9. E. Vivier, J. A. Nunes and F. Vely, *Science*, 2004, **306**, 1517-1519.
10. T. A. Fehniger, M. A. Cooper, G. J. Nuovo, M. Cella, F. Facchetti, M. Colonna and M. A. Caligiuri, *Blood*, 2003, **101**, 3052-3057.
11. G. Ferlazzo, D. Thomas, S. L. Lin, K. Goodman, B. Morandi, W. A. Muller, A. Moretta and C. Munz, *J Immunol*, 2004, **172**, 1455-1462.
12. A. Nagler, L. L. Lanier, S. Cwirla and J. H. Phillips, *J Immunol*, 1989, **143**, 3183-3191.
13. A. Nagler, L. L. Lanier and J. H. Phillips, *J Exp Med*, 1990, **171**, 1527-1533.
14. K. B. Nguyen, T. P. Salazar-Mather, M. Y. Dalod, J. B. Van Deusen, X. Q. Wei, F. Y. Liew, M. A. Caligiuri, J. E. Durbin and C. A. Biron, *J Immunol*, 2002, **169**, 4279-4287.
15. M. A. Cooper, T. A. Fehniger, S. C. Turner, K. S. Chen, B. A. Ghaheri, T. Ghayur, W. E. Carson and M. A. Caligiuri, *Blood*, 2001, **97**, 3146-3151.
16. T. A. Fehniger, M. H. Shah, M. J. Turner, J. B. VanDeusen, S. P. Whitman, M. A. Cooper, K. Suzuki, M. Wechser, F. Goodsaid and M. A. Caligiuri, *J Immunol*, 1999, **162**, 4511-4520.
17. J. Gosselin, A. TomoIu, R. C. Gallo and L. Flamand, *Blood*, 1999, **94**, 4210-4219.
18. E. Marcenaro, M. Della Chiesa, F. Bellora, S. Parolini, R. Millo, L. Moretta and A. Moretta, *J Immunol*, 2005, **174**, 3992-3998.
19. S. Ushio, M. Namba, T. Okura, K. Hattori, Y. Nukada, K. Akita, F. Tanabe, K. Konishi, M. Micallef, M. Fujii, K. Torigoe, T. Tanimoto, S. Fukuda, M. Ikeda, H. Okamura and M. Kurimoto, *J Immunol*, 1996, **156**, 4274-4279.
20. D. M. Andrews, M. J. Estcourt, C. E. Andoniou, M. E. Wikstrom, A. Khong, V. Voigt, P. Fleming, H. Tabarias, G. R. Hill, R. G. van der Most, A. A. Scalzo, M. J. Smyth and M. A. Degli-Esposti, *J Exp Med*, 2010, **207**, 1333-1343.
21. G. Ferlazzo, M. L. Tsang, L. Moretta, G. Melioli, R. M. Steinman and C. Munz, *J Exp Med*, 2002, **195**, 343-351.
22. D. Piccioli, S. Sbrana, E. Melandri and N. M. Valiante, *J Exp Med*, 2002, **195**, 335-341.
23. P. A. Lang, K. S. Lang, H. C. Xu, M. Grusdat, I. A. Parish, M. Recher, A. R. Elford, S. Dhanji, N. Shaabani, C. W. Tran, D. Dissanayake, R. Rahbar, M. Ghazarian, A. Brustle, J. Fine, P. Chen, C. T. Weaver, C. Klose, A. Diefenbach, D. Haussinger, J. R. Carlyle, S. M. Kaech, T. W. Mak and P. S. Ohashi, *Proc Natl Acad Sci U S A*, 2012, **109**, 1210-1215.
24. S. N. Waggoner, M. Cornberg, L. K. Selin and R. M. Welsh, *Nature*, 2011, **481**, 394-398.

25. R. Jacobs, G. Hintzen, A. Kemper, K. Beul, S. Kempf, G. Behrens, K. W. Sykora and R. E. Schmidt, *Eur J Immunol*, 2001, **31**, 3121-3127.
26. K. Juelke, M. Killig, M. Luetke-Eversloh, E. Parente, J. Gruen, B. Morandi, G. Ferlazzo, A. Thiel, I. Schmitt-Knosalla and C. Romagnani, *Blood*, 2010, **116**, 1299-1307.
27. J. Yu, H. C. Mao, M. Wei, T. Hughes, J. Zhang, I. K. Park, S. Liu, S. McClory, G. Marcucci, R. Trotta and M. A. Caligiuri, *Blood*, 2010, **115**, 274-281.
28. F. J. Culley, M. Johnson, J. H. Evans, S. Kumar, R. Crilly, J. Casasbuenas, T. Schnyder, M. Mehrabi, M. P. Deonarain, D. S. Ushakov, V. Braud, G. Roth, R. Brock, K. Kohler and D. M. Davis, *PLoS Biol*, 2009, **7**, e1000159.
29. C. Wulfing, B. Purtic, J. Klem and J. D. Schatzle, *Proc Natl Acad Sci U S A*, 2003, **100**, 7767-7772.
30. K. Guldevall, B. Vanherberghen, T. Frisk, J. Hurtig, A. E. Christakou, O. Manneberg, S. Lindstrom, H. Andersson-Svahn, M. Wiklund and B. Onfelt, *PLoS One*, 2010, **5**, e15453.
31. R. Bhat and C. Watzl, *PLoS One*, 2007, **2**, e326.
32. M. A. Khorshidi, B. Vanherberghen, J. M. Kowalewski, K. R. Garrod, S. Lindstrom, H. Andersson-Svahn, H. Brismar, M. D. Cahalan and B. Onfelt, *Integr Biol (Camb)*, 2011, **3**, 770-778.
33. J. E. Snyder, W. J. Bowers, A. M. Livingstone, F. E. Lee, H. J. Federoff and T. R. Mosmann, *Nat Med*, 2003, **9**, 231-235.
34. Q. Han, N. Bagheri, E. M. Bradshaw, D. A. Hafler, D. A. Lauffenburger and J. C. Love, *Proc Natl Acad Sci U S A*, 2012, **109**, 1607-1612.
35. Q. Han, E. M. Bradshaw, B. Nilsson, D. A. Hafler and J. C. Love, *Lab Chip*, 2010, **10**, 1391-1400.
36. N. Varadarajan, B. Julg, Y. J. Yamanaka, H. Chen, A. O. Ogunniyi, E. McAndrew, L. C. Porter, A. Piechocka-Trocha, B. J. Hill, D. C. Douek, F. Pereyra, B. D. Walker and J. C. Love, *J Clin Invest*, 2011, **121**, 4322-4331.
37. J. C. Love, J. L. Ronan, G. M. Grotenbreg, A. G. van der Veen and H. L. Ploegh, *Nat Biotechnol*, 2006, **24**, 703-707.
38. A. O. Ogunniyi, C. M. Story, E. Papa, E. Guillen and J. C. Love, *Nat Protoc*, 2009, **4**, 767-782.
39. N. Varadarajan, D. S. Kwon, K. M. Law, A. O. Ogunniyi, M. N. Anahtar, J. M. Richter, B. D. Walker and J. C. Love, *Proc Natl Acad Sci U S A*, 2012, **109**, 3885-3890.
40. G. Alter, J. M. Malenfant and M. Altfeld, *J Immunol Methods*, 2004, **294**, 15-22.
41. M. R. Betts, J. M. Brenchley, D. A. Price, S. C. De Rosa, D. C. Douek, M. Roederer and R. A. Koup, *J Immunol Methods*, 2003, **281**, 65-78.
42. C. Tomescu, J. Chehimi, V. C. Maino and L. J. Montaner, *J Leukoc Biol*, 2009, **85**, 871-876.
43. D. D. Taub, T. J. Sayers, C. R. Carter and J. R. Ortaldo, *J Immunol*, 1995, **155**, 3877-3888.
44. T. Dragic, V. Litwin, G. P. Allaway, S. R. Martin, Y. Huang, K. A. Nagashima, C. Cayanan, P. J. Maddon, R. A. Koup, J. P. Moore and W. A. Paxton, *Nature*, 1996, **381**, 667-673.
45. F. Cocchi, A. L. DeVico, A. Garzino-Demo, S. K. Arya, R. C. Gallo and P. Lusso, *Science*, 1995, **270**, 1811-1815.
46. K. Schroder, P. J. Hertzog, T. Ravasi and D. A. Hume, *J Leukoc Biol*, 2004, **75**, 163-189.
47. J. S. Orange, *Microbes Infect*, 2002, **4**, 1545-1558.

48. J. Deguine, B. Breart, F. Lemaitre, J. P. Di Santo and P. Bousso, *Immunity*, 2010, **33**, 632-644.
49. M. Nieto, F. Navarro, J. J. Perez-Villar, M. A. del Pozo, R. Gonzalez-Amaro, M. Mellado, J. M. Frade, A. C. Martinez, M. Lopez-Botet and F. Sanchez-Madrid, *J Immunol*, 1998, **161**, 3330-3339.
50. K. R. Garrod, S. H. Wei, I. Parker and M. D. Cahalan, *Proc Natl Acad Sci U S A*, 2007, **104**, 12081-12086.
51. S. L. Spencer, S. Gaudet, J. G. Albeck, J. M. Burke and P. K. Sorger, *Nature*, 2009, **459**, 428-432.
52. J. A. Trapani and M. J. Smyth, *Nat Rev Immunol*, 2002, **2**, 735-747.
53. C. Lehmann, M. Zeis and L. Uharek, *Br J Haematol*, 2001, **114**, 660-665.
54. T. H. Landowski, K. H. Shain, M. M. Oshiro, I. Buyuksal, J. S. Painter and W. S. Dalton, *Blood*, 1999, **94**, 265-274.
55. A. H. Montel, M. R. Bochan, J. A. Hobbs, D. H. Lynch and Z. Brahmi, *Cell Immunol*, 1995, **166**, 236-246.
56. R. Munker, F. Marini, S. Jiang, C. Savary, L. Owen-Schaub and M. Andreeff, *Hematol Cell Ther*, 1997, **39**, 75-78.
57. V. Hietakangas, M. Poukkula, K. M. Heiskanen, J. T. Karvinen, L. Sistonen and J. E. Eriksson, *Mol Cell Biol*, 2003, **23**, 1278-1291.
58. A. Chauveau, A. Aucher, P. Eissmann, E. Vivier and D. M. Davis, *Proc Natl Acad Sci U S A*, 2010, **107**, 5545-5550.
59. S. E. Henrickson, T. R. Mempel, I. B. Mazo, B. Liu, M. N. Artyomov, H. Zheng, A. Peixoto, M. P. Flynn, B. Senman, T. Junt, H. C. Wong, A. K. Chakraborty and U. H. von Andrian, *Nat Immunol*, 2008, **9**, 282-291.
60. E. Reefman, J. G. Kay, S. M. Wood, C. Offenhauser, D. L. Brown, S. Roy, A. C. Stanley, P. C. Low, A. P. Manderson and J. L. Stow, *J Immunol*, 2010, **184**, 4852-4862.
61. Z. B. Kurago, C. T. Lutz, K. D. Smith and M. Colonna, *J Immunol*, 1998, **160**, 1573-1580.
62. D. G. Hesslein, R. Takaki, M. L. Hermiston, A. Weiss and L. L. Lanier, *Proc Natl Acad Sci U S A*, 2006, **103**, 7012-7017.
63. D. D. Billadeau, J. L. Upshaw, R. A. Schoon, C. J. Dick and P. J. Leibson, *Nat Immunol*, 2003, **4**, 557-564.
64. J. G. Egen, A. G. Rothfuchs, C. G. Feng, M. A. Horwitz, A. Sher and R. N. Germain, *Immunity*, 2011, **34**, 807-819.
65. D. M. Davis, *Nat Rev Immunol*, 2009, **9**, 543-555.
66. M. Sips, G. Sciaranghella, T. Diefenbach, A. S. Dugast, C. T. Berger, Q. Liu, D. Kwon, M. Ghebremichael, J. D. Estes, M. Carrington, J. N. Martin, S. G. Deeks, P. W. Hunt and G. Alter, *Mucosal Immunol*, 2012, **5**, 30-40.
67. P. Bonorino, M. Ramzan, X. Camous, T. Dufeu-Duchesne, M. A. Thelu, N. Sturm, A. Dariz, C. Guillermet, M. Pernollet, J. P. Zarski, P. N. Marche, V. Leroy and E. Jouvin-Marche, *J Hepatol*, 2009, **51**, 458-467.

Figure legends

Fig. 1 NK cells interrogate and lyse K562 target cells when co-incubated in nanowells. (A) Schematic of the single-cell cytolysis (SCC) assay. NK cells and K562 target cells are loaded onto an array of nanowells. An initial set of images is acquired to determine the number of cells per well; after 4 h of incubation, a second set of images is acquired to identify wells in which a killing event occurred ($SYTOX^+$ target cell). (B) Representative images of NK cells (blue) co-incubated with target cells (red) in the nanowells. Lysed target cells become positive for SYTOX (green). (C) Frequencies of cytolytic events measured by the SCC assay and of degranulated NK cells measured by flow cytometry after 4 h of NK cell-target cell interactions. NK cells were incubated for 20 h with the indicated stimulation conditions prior to either assay. Data from the SCC assay were gated to include wells containing a single NK cell and a single target. Target cell-induced degranulation is expressed as ΔCD107a, which indicates the difference in expression of CD107a on the surface of NK cells that were or were not exposed to target cells in bulk. Mean and standard deviation (SD) for at least three donors per condition are shown. ###$P < .0001$, Chi-squared with Yate's correction comparison of lysis rates of target cells in wells on the same array containing zero NK cells (background death) or one NK cell. *$P < .05$, **$P < .01$, ***$P < .001$, one-way ANOVA followed by Tukey's post-test.

Fig. 2 NK cells act independently when lysing a single target cell in a nanowell. (A) Representative distribution of SYTOX intensity in target cells after being co-incubated for 4 h in nanowells with one, two, or three NK cells. Data were gated to include wells containing a single target cell. Example images show the initial occupancy of the nanowells for each combination. The percentage of lysed target cells (double-positive for SYTOX and CellTracker Red) is indicated. In this example, the NK cells were obtained from the donor depicted in gold in the plots in Panel B and were activated with IFN-α plus IL-2. MFI, median fluorescence intensity. (B) Observed frequencies of cytolysis (filled circles; colors indicate unique donors) in nanowells containing 0–3 NK cells. For each donor, the frequencies of cytolysis predicted from the frequency observed in wells containing a single NK cell are shown as dotted lines. Prior to the assay, NK cells were stimulated with the indicated conditions for 20 h.

Fig. 3 Dynamic cytolytic interactions between NK cells and target cells. (A) Representative composite micrographs of a single IL-2-activated (50 U/mL, 44 h) NK cell (blue) interacting with a target cell (red) and inducing cytolysis (green; SYTOX). Images were acquired every 8 min for 4 h. For each target cell, the SYTOX intensity and the distance to the NK cell were calculated using automated tracking scripts. (B) Distribution of the number of contacts formed by single NK cells with distinct target cells over 4 h as a function of the total number of target cells residing in each nanowell. (C) Histogram of the total NK cell-target cell contact time required for cytolytic NK cells to induce the permeabilization of the membrane of the target cell. Data are segregated into pairs of NK cells and target cells that were not yet in contact in the first image (dark grey bars) or were already in contact in the first image (light grey bars). (D) Relative probability of an NK cell lysing the first, second, third, or fourth target cell that it encountered. Groups are segregated based on the total number of distinct target cells that were encountered, and relative probabilities were calculated as the fraction of lysed target cells in each group that were the n^{th} target cell to be contacted by the NK cell. Panels A–C are representative of two independent donors; Panel D shows combined data from both donors.

Fig. 4 Microengraving measures the short-term secretory activity of individual NK cells. (A) Schematic of microengraving to detect secreted cytokines and chemokines. A capture antibody-coated glass slide is placed in contact and incubated with the array of nanowells; this process creates a matched microarray of secreted proteins that is subsequently detected with fluorescently labeled antibodies, imaged, and analyzed to correlate secretion events to the nanowell of origin. (B) Representative matched images measuring cytolytic activity and the secretion of proteins from the same NK cell. Labeling is as described in Fig. 1B. (C) Production of cytokines and chemokines measured by microengraving or intracellular cytokine staining (ICS). NK cells were incubated for 20 h with the indicated stimulation conditions prior to either assay and then incubated with target cells in the nanowells (microengraving assay) or in bulk (ICS assay) for 4 h. The microengraving data were gated to include wells containing a single NK cell and multiple target cells. Mean and SD for at least three donors per condition are shown. Note difference in scale between the two graphs.

Fig. 5 Secretion of IFN-γ is associated with the velocity of NK cells during contact with target cells. (A) Representative composite micrographs of IL-2-activated (50 U/ml, 44 h) NK cell-target cell interactions and corresponding measurements of secreted chemokines and cytokines. Interactions were tracked for 4 h at 8 min intervals using time-lapse microscopy (labeling as described in Fig. 3A); microengraving was performed immediately afterward for 2 h to capture chemokines and cytokines secreted by each NK cell. Micrographs in rows 1–3 correspond to Supplementary Videos 1–3. (B) Secretion of MIP-1β and IFN-γ from single NK cells. NK cells are segregated based on whether they contacted a target cell, and, if they did contact at least one target cell, whether they exhibited cytolytic activity. Dashed lines indicate the threshold for positive secretion events (background + 2 SD). $^{**}P < .01$, $^{***}P < .001$, n.s., not significant, Mann-Whitney test. (C) Mean velocities of NK cells in nanowells in the absence of target cells (0 K562), during contact with target cells, and after contact with target cells. $^{***}P < .001$, Kruskal-Wallis test followed by Dunn's post-test. (D) Mean velocities of NK cells in nanowells during contact with target cells. Data are segregated by functional outcome. $^{*}P < .05$, n.s., not significant, Mann-Whitney test. In Panels B–D the mean and standard error of the mean (SEM) are indicated in red. (E) Tracks of NK cells in the absence of target cells (left) or during contact with a target cell (right). The tracks during contact are segregated by secretory outcome. Each plot displays n = 15 tracks that were randomly selected from the pool of all eligible cell tracks. All results are representative of two independent donors.

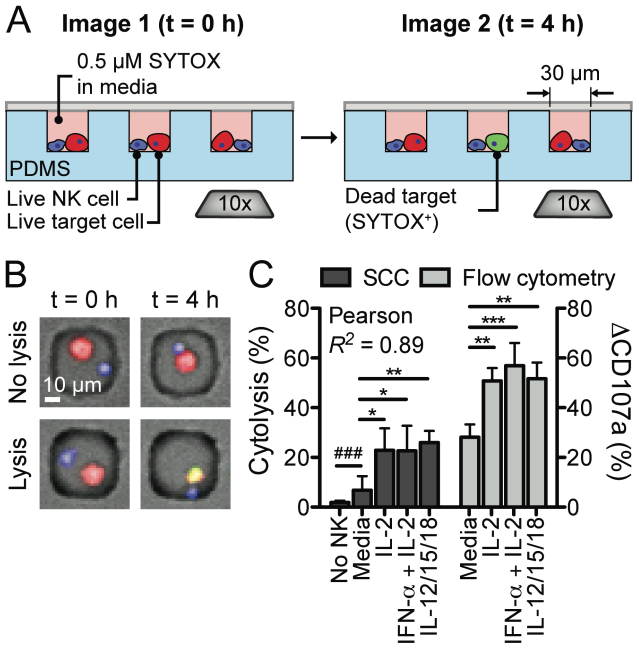
A
Image 1 (t = 0 h)
Image 2 (t = 4 h)
0.5 μM SYTOX
in media
30 μm
PDMS
Live NK cell
Live target cell
10x
Dead target
(SYTOX+)
10x
B
t = 0 h
t = 4 h
No lysis
Lysis
10 μm
C
SCC
Flow cytometry
Pearson
R2 = 0.89
Cytolysis (%)
ΔCD107a (%)
No NK
Media
IL-2
IFN-α + IL-2
IL-12/15/18
Media
IL-2
IFN-α + IL-2
IL-12/15/18

Figure 1

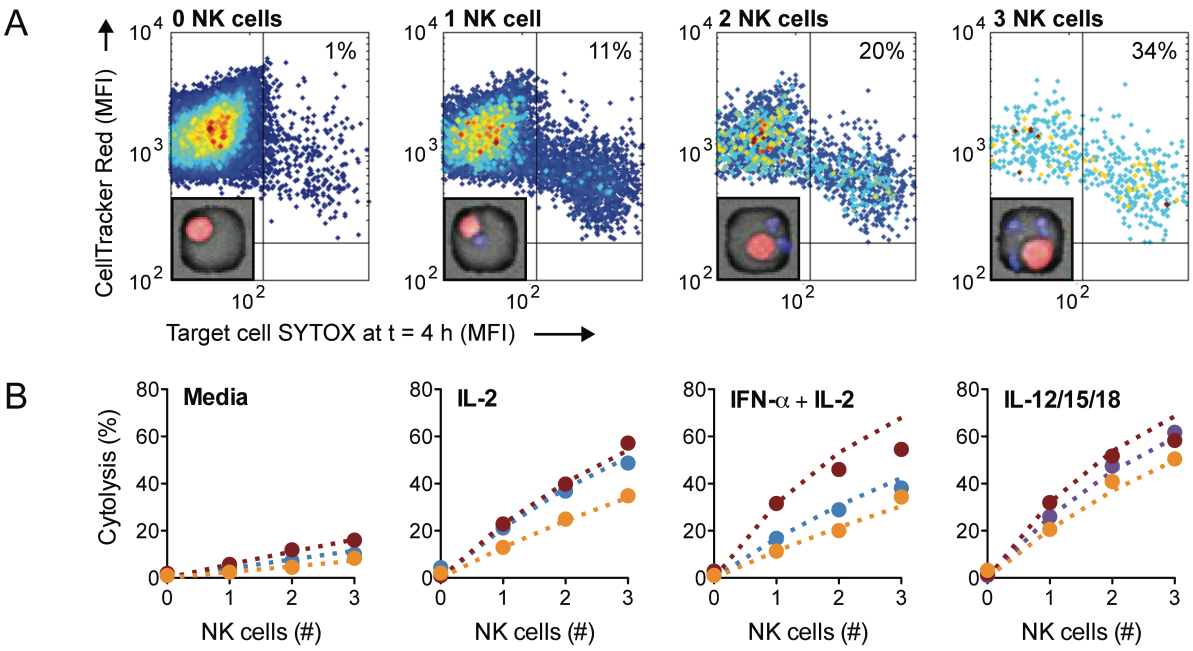
A
0 NK cells
1%
1 NK cell
11%
2 NK cells
20%
3 NK cells
34%
CellTracker Red (MFI)
Target cell SYTOX at t = 4 h (MFI)
B
Media
IL-2
IFN-α + IL-2
IL-12/15/18
Cytolysis (%)
NK cells (#)

Figure 2

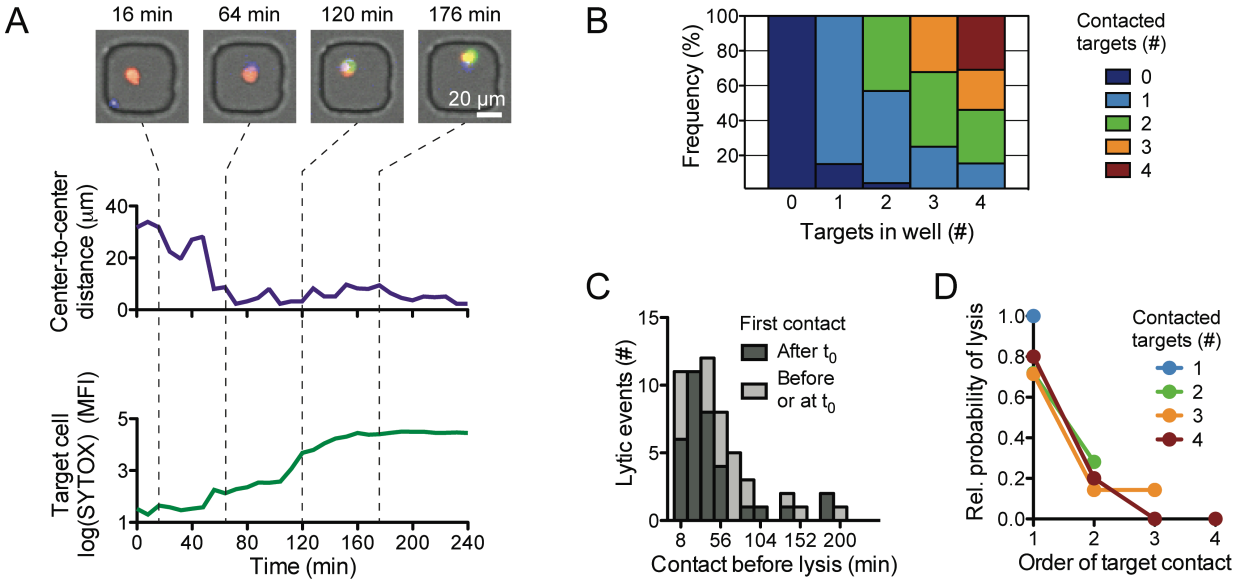
A
16 min
64 min
120 min
176 min
20 µm
Center-to-center distance (µm)
Target cell log(SYTOX) (MFI)
Time (min)
B
Frequency (%)
Targets in well (#)
Contacted targets (#)
0
1
2
3
4
C
Lytic events (#)
First contact
After t0
Before or at t0
Contact before lysis (min)
D
Rel. probability of lysis
Contacted targets (#)
Order of target contact

Figure 3

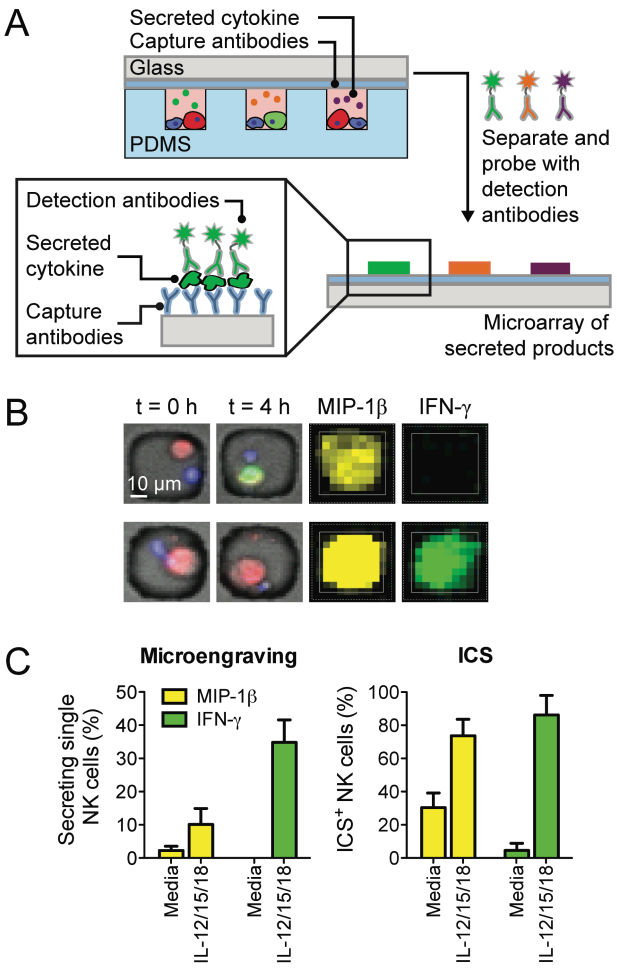
A
Secreted cytokine
Capture antibodies
Glass
PDMS
Separate and probe with detection antibodies
Detection antibodies
Secreted cytokine
Capture antibodies
Microarray of secreted products
B
t = 0 h
t = 4 h
MIP-1β
IFN-γ
10 μm
C
Microengraving
ICS
Secreting single NK cells (%)
ICS+ NK cells (%)
MIP-1β
IFN-γ
Media
IL-12/15/18

Figure 4

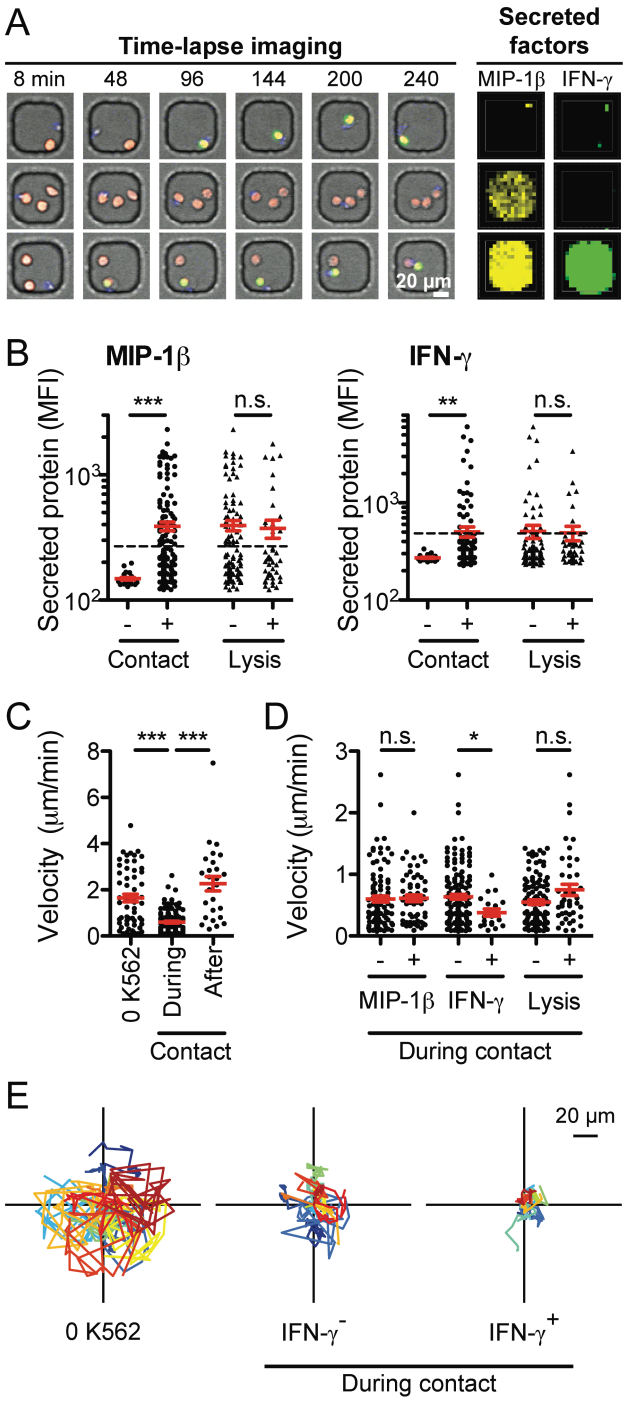
A
Time-lapse imaging
8 min
48
96
144
200
240
20 µm
Secreted factors
MIP-1β
IFN-γ
B
MIP-1β
IFN-γ
Secreted protein (MFI)
***
n.s.
**
Contact
Lysis
C
Velocity (µm/min)
0 K562
During
After
Contact
D
n.s.
*
MIP-1β
IFN-γ
Lysis
During contact
E
20 µm
0 K562
IFN-γ-
IFN-γ+
During contact

Figure 5

Supplementary information for:

Single-cell analysis of the dynamics and functional outcomes of interactions between human natural killer cells and target cells

Yvonne J. Yamanaka,[1] Christoph T. Berger,[2] Magdalena Sips,[2] Patrick C. Cheney,[2] Galit Alter,[2] and J. Christopher Love[2-4]

[1]*Department of Biological Engineering, Massachusetts Institute of Technology, 77 Massachusetts Ave., Cambridge, MA 02139*

[2]*The Ragon Institute of MGH, MIT, and Harvard, Charlestown Navy Yard, Boston, MA 02129*

[3]*Department of Chemical Engineering, Massachusetts Institute of Technology, 77 Massachusetts Ave., Cambridge, MA 02139*

[4]*Koch Institute for Integrative Cancer Research, 77 Massachusetts Ave., Bldg. 76-253, Cambridge, MA 02139*

Correspondence should be addressed to:

J. Christopher Love, Ph.D.
Department of Chemical Engineering
Koch Institute for Integrative Cancer Research
Massachusetts Institute of Technology
77 Massachusetts Ave., Bldg. 76-253
Cambridge, MA 02139
Phone: 617-324-2300
Fax: 617-258-5042
Email: clove@mit.edu

Supplemental methods

Fabrication of arrays of nanowells

Arrays of nanowells containing either 30 μm (248,832 wells/array) or 50 μm (84,672 wells/array) cubic wells were prepared on 75 × 25 mm^2 glass slides (Corning) by injecting a silicone elastomer (poly(dimethylsiloxane) (PDMS; Dow Corning), 10:1 ratio of base:catalyst) into a mold containing a microfabricated silicon master. PDMS was cured at 80°C for 4 h and then released from the mold. Shortly before depositing cells into the array, the arrays were treated with an oxygen plasma (Harrick PDC-32G) for 30 s to sterilize the array and render the PDMS hydrophilic. Arrays were stored in phosphate-buffered saline (PBS) until use, and were washed with complete media prior to cell loading.

Microengraving to detect secreted proteins

Capture antibodies against MIP-1β (R&D Systems), IFN-γ (Mabtech), and human immunoglobulin G (hIgG) (ZyMax; Invitrogen) (10 μg/mL each in borate buffer; pH 9) were coated onto poly(L-lysine)-coated glass microscope slides for 1 h at room temperature. Slides were then blocked in 1.5% bovine serum albumin (BSA; EMD Chemicals) / PBS-TWEEN20 (0.05%; Sigma-Aldrich) (PBST) for 30 min, washed once in PBS, dipped in water, and spun dry. Prior to microengraving, the cell-loaded arrays of nanowells were rinsed with serum-free media containing hIgG (34.5 ng/mL; Athens Research & Technology) to provide a positive background signal in every well and facilitate the registration of the features during image analysis of the captured protein microarrays. Excess media was aspirated and the capture antibody-coated glass slides were placed face down on top of the cell-loaded arrays (Fig. 4A). Compression was applied using a microarray hybridization chamber (Agilent). The clamped arrays were incubated for 1 h (30 μm wells) or 2 h (50 μm wells) to allow the capture of secreted proteins onto the antibody-coated glass slide. The resulting microarrays of secreted proteins were then separated from the PDMS array, washed in PBS, blocked with 1.5% BSA-PBST, and hybridized (45 min, room temperature) with the following detection antibodies: biotinylated anti-MIP-1β, anti-IFN-γ-AlexaFluor555, and anti-hIgG-AlexaFluor700 (1 μg/mL each in 0.1% BSA-PBST, all from same manufacturers as corresponding capture antibodies). Arrays were washed in PBS and PBST and then hybridized an additional 30 min at room temperature with streptavidin-AlexaFluor647 (1

μg/mL; Invitrogen). After a final series of washes in PBS, PBST, and water, the protein microarrays were dried and imaged with 5-μm resolution using a commercial microarray scanner (GenePix 4200AL, Molecular Devices).

The microarray of secreted proteins was analyzed using commercial image processing software (GenePix Pro 6, Molecular Devices). The median fluorescence intensity (MFI) in each channel was calculated for each spot in the array to determine the relative intensity of secretion of the cells in the corresponding nanowell. Data were filtered to exclude spots with saturated pixels or high coefficients of variation (>70–90). Spots with a high signal-to-noise ratio (>3–5), low relative local background, and MFI > [global background + 2 standard deviations] were marked as positive spots.

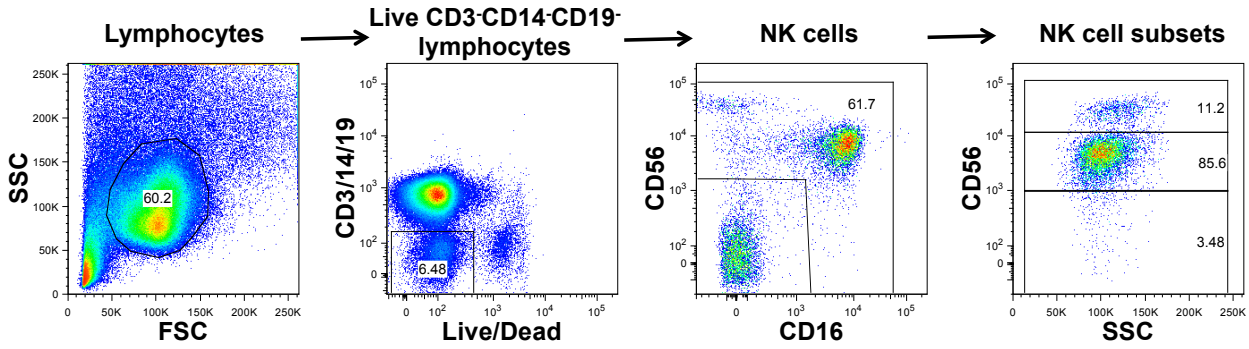

Fig. S1 Flow cytometry gating scheme for NK cells. Numbers indicate percentages within each gate. NK cells were defined as live $CD3^-CD14^-CD19^-$ lymphocytes expressing CD56 and/or CD16 (i.e., $CD56^+CD16^-$ ($CD56^{bright}$ NK cells), $CD56^+CD16^+$ ($CD56^{dim}$ NK cells) or $CD56^-CD16^+$ ($CD56^{neg}$ NK cells)).

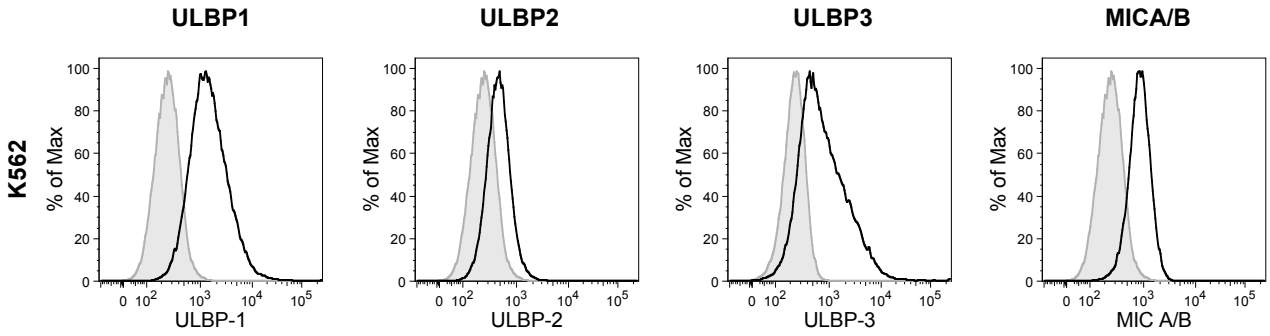

Fig. S2 Surface expression of NKG2D ligands on K562 target cells. Black lines represent the K562 cells stained with the indicated antibody; grey shaded areas show the respective isotype controls.

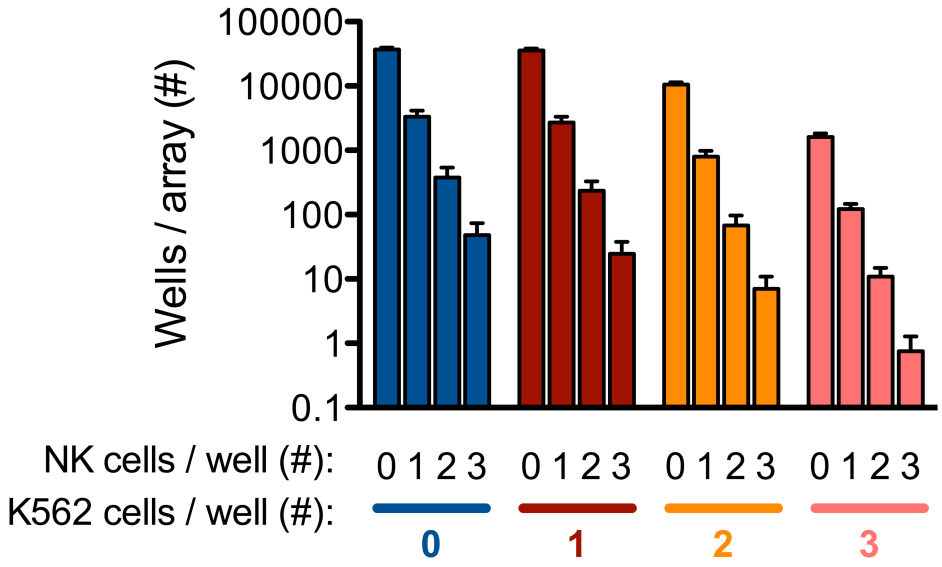

Fig. S3 Distribution of NK cells and K562 target cells in arrayed nanowells. Bar graph of the mean and standard deviation (SD) of the numbers of nanowells on each array that contained the indicated combinations of NK cells and target cells. Results were compiled from eight arrays containing 30 μm cubic nanowells. Each 75 × 25 mm^2 array contained 248,832 wells. In all experiments, to minimize any potential edge effects, only wells located in the center of the array were considered (147,456 wells). Further filtering was performed to exclude wells with dead cells at the t = 0 h time-point and wells in which the cell occupancy changed between the images acquired at t = 0 h and t = 4 h.

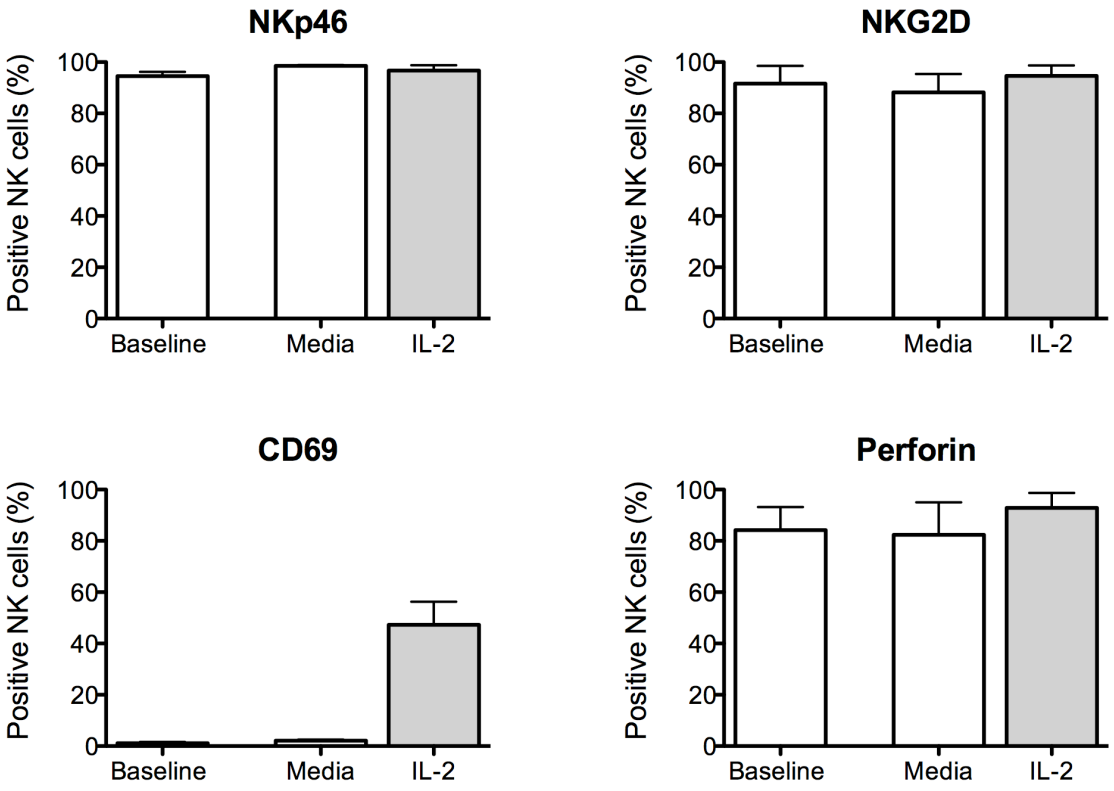

Fig. S4 Phenotypes of NK cells after 44 h stimulation with IL-2. NKp46, NKG2D, CD69, and intracellular perforin were measured by flow cytometry for freshly isolated NK cells (Baseline) or for NK cells stimulated for 44 h in media or in 50 U/ml IL-2. Bar graphs show mean and SD for three donors per condition.